


## Comparison of the static structure factor at long wavelengths for a dusty plasma liquid and other liquids

Vitaliy Zhuravlyov \* and J. Goree


*Department of Physics and Astronomy, University of Iowa, Iowa City, Iowa 52242, USA*

Jack F. Douglas

*Materials Science and Engineering Division, National Institute of Standards and Technology, Gaithersburg, Maryland 20899, USA*

Paolo Elvati  and Angela Violi

*Department of Mechanical Engineering, University of Michigan, Ann Arbor, Michigan 48109, USA*

 (Received 28 August 2021; revised 30 August 2022; accepted 23 October 2022; published 28 November 2022)

Especially small values of the static structure factor  $S(k)$  at long wavelengths, i.e., small  $k$ , were obtained in an analysis of experimental data, for a two-dimensional dusty plasma in its liquid state. For comparison, an analysis of  $S(k)$  data was carried out for many previously published experiments with other liquids. The latter analysis indicates that the magnitude of  $S(k)$  at small  $k$  is typically in a range 0.02–0.13. In contrast, the corresponding value for a dusty plasma liquid was found to be as small as 0.0139. Another basic finding for the dusty plasma liquid is that  $S(k)$  at small  $k$  generally increases with temperature, with its lowest value, noted above, occurring near the melting point. Simulations were carried out for the dusty plasma liquid, and their results are generally consistent with the experiment. Since a dusty plasma has a soft interparticle interaction, our findings support earlier theoretical suggestions that a useful design strategy for creating materials having exceptionally low values of  $S(0)$ , so-called hyperuniform materials, is the use of a condensed material composed of particles that interact softly at their periphery.

DOI: [10.1103/PhysRevE.106.055212](https://doi.org/10.1103/PhysRevE.106.055212)

### I. INTRODUCTION

The static structure factor  $S(k)$  has long been studied experimentally as a measure of the microscopic structure of liquids [1–3], averaged over a finite sample size. A Fourier transform relates  $S(k)$  to the pair correlation function  $g(r)$ , which measures the probability of two particles being separated by a given distance  $r$ .

While the  $S(k)$  curve has several prominent peaks at large values of the Fourier transform variable  $k$ , here we will be concerned mainly with the value of  $S(k)$  at values of  $k$  much smaller than for any of the peaks. In the limiting case of  $k \rightarrow 0$ ,  $S(0)$  is proportional to isothermal compressibility [1–3], and it is a measure of a substance’s closeness to hyperuniformity, which is a theoretical condition where density fluctuations are suppressed at long wavelengths [4]. It has been predicted that hyperuniform substances can have unusual mechanical, transport, and optical properties, for example stealthy scattering patterns [5]. These predictions, which are beyond the scope of the present work, have led to a great interest recently in searching for a path to hyperuniformity in physical substances [5–19], as discussed further in the Supplemental Material [20].

Experimental measurements of  $S(k)$  in liquids have been reported since at least the 1960s, when diffraction

measurements of liquid metals became common [26]. Many original experimental reports included graphs of  $S(k)$ , over a range of  $k$  values including the small  $k$  values that are the focus of the present paper. In our literature search, however, we did not find much quantitative analysis of the value of  $S(k)$  at small  $k$ . The previous experiments used liquids composed of various substances, but we did not find remarks in the literature to indicate a typical value of  $S(k)$  at small  $k$  for a liquid, nor did we find a comparison of values for various substances. In this paper, we will provide such a comparison, and determine a general range of values that are typical for various liquids. This comparison will be based on 22 separate reports of experimental  $S(k)$  data, published over several decades describing 27 experiments with 24 substances. These substances include liquid metals made of 15 different elements [26–37] and other atomic liquids [38–42] composed of He, Kr, and Cl. Our comparison also included experiments with colloids, which used diffraction [43,44] or imaging [19,45,46] to obtain  $S(k)$ . To keep our study of manageable proportions, we limit our scope to liquids, and do not include, for example, amorphous solids and glasses in our survey of previous experiments. With our emphasis on experiments, we do not survey previous simulation studies of  $S(k)$ .

Our comparisons in this paper will include an analysis that we carried out to obtain  $S(k)$  for a dusty plasma liquid. For this purpose, we use data from the dusty plasma experiment by Haralson and Goree [47,48], which we denote as HG. We

\*vitaliy-zhuravlyov@uiowa.edu

will explain how we obtained  $S(k)$  for that experiment and for a simulation that models the experiment of HG.

A direct experimental measurement of the limiting value  $S(0)$  is, in general, impractical. When diffraction is used to obtain  $S(k)$ , there is an unscattered beam at zero scattering angle, and that unscattered beam obscures the diffraction pattern [49] for a range of small values of  $k$ . When direct imaging of particles is used, as in some colloidal liquids and dusty plasmas, the sample size is finite, so that Fourier transforms do not extend to zero value of  $k$ .

Extrapolation is one approach used by a few authors to estimate  $S(0)$  based on their experimentally obtained  $S(k)$  curves [27,39,45,50] at finite  $k$ . These extrapolations have been done with ad hoc approaches that vary from one paper to another, and are sometimes not described exactly. We are unaware of a theoretically justified extrapolation algorithm that is applicable for all experiments. For this reason, we seek another approach to report  $S(k)$  at small  $k$ , which will work well when analyzing data from many kinds of experiments.

The measure we adopt here for the analysis of experimentally measured curves of  $S(k)$  is simply the selection of the lowest data point on that curve. We denote this value  $S_{\min}$ . The corresponding data point is always found at small  $k$ , well below the first peak of  $S(k)$ . In the absence of experimental noise or artifacts in the  $S(k)$  curve,  $S_{\min}$  would be somewhat larger than the limiting value  $S(0)$ .

For the purpose of discussing closeness to hyperuniformity, we also need a practical measure of the hyperuniformity index. That index has been defined [5,51] as  $H \equiv S(0)/S_{\text{peak}}$ , where  $S_{\text{peak}}$  is the height of the first peak of  $S(k)$ . For this purpose, we again avoid extrapolations of  $S(k)$  measurements to yield an estimate of  $S(0)$ ; instead, when comparing measurements of different substances, we report the ratio  $S_{\min}/S_{\text{peak}}$ .

In our analysis of  $S(k)$  for previous experiments, we will consider in detail the dusty plasma experiment of HG [47,48]. A dusty plasma, which is sometimes called a complex plasma, is a collection of small electrically charged particles of solid matter that are immersed in a partially ionized gas containing electrons, ions, and neutral atoms [52–55]. The solid particles are called dust particles as in astronomy [56]. In laboratory experiments, particles with a diameter of a few  $\mu\text{m}$  typically have a charge of many thousands of electrons. Random motion of the dust particles can be described by a kinetic temperature  $T$ . Due to the nonequilibrium character of a laboratory plasma, the dust kinetic temperature is not equal to other temperatures in the system, including the temperatures of electrons, ions, and the surface temperature of a particle. The dust particles interact among themselves with a screened Coulomb repulsion, which is a particularly soft interaction that is often idealized in models as a Yukawa or Debye-Hückel potential [57]. The Yukawa potential is defined as  $(Q^2/4\pi\epsilon_0 r)\exp(-r/\lambda)$ , where  $Q$  is a particle charge,  $r$  is the distance between a pair of particles, and  $\lambda$  is a screening length. The screening, in a dusty plasma, arises due to nearby electrons and ions so that  $\lambda$  is independent of the dust kinetic temperature  $T$ .

When the particle charges in a dusty plasma are as large as thousands of electrons, the interparticle potential energy becomes quite large and greatly exceeds the thermal kinetic energy of dust particles. Under this condition, called strong

coupling in the plasma physics literature [58–61], dust particles tend to self-organize and sustain a solidlike or liquidlike microscopic structure [62–65], unlike the more disordered gaslike conditions of the more common weakly coupled plasmas [66,67]. Because of the softness of its interparticle interaction and a large interparticle spacing, a dusty plasma in the solid phase has a shear modulus that is 19 orders of magnitude less than for metals [68]. There are several theoretical models of strongly coupled plasmas, with varying degrees of applicability to experiment. Among the simplest models is the OCP (one-component plasma) description, which neglects the rather important ability of ions and electrons to move about, for example, in response to the charged dust particles [55]. In this OCP approximation,  $S(k)$  in the  $k \rightarrow 0$  limit diminishes quadratically with  $k$  to a value of exactly zero [58,69–71].

Dusty plasmas are well suited for the experimental study of microscopic structure and correlations. The cloud of dust particles is suspended electrically, without any frictional contact with a solid surface.

In some experiments, the cloud is shaped as a single horizontal layer, so that it behaves as a two-dimensional (2D) substance [72–77]. Direct imaging of the dust particles in a 2D layer is practical using video microscopy [78], which has made possible experimental studies of phenomena such as superdiffusion [79,80], dynamical heterogeneity [81], and a violation of the Stokes-Einstein relation [82]. Many other phenomena have been studied as well, which is also the case for a dusty plasma's close relative, charged colloid particle suspensions [83]. Unlike colloids, however, dusty plasmas are generally underdamped, and they allow easy adjustment of the kinetic temperature using an energy input such as laser heating [84–86]. In this way, a strongly coupled 2D dusty plasma in its solid phase can be melted. For the melting point  $T_m$ , we will rely on data obtained using 2D Yukawa simulations by Hartmann *et al.* [87]. (We also mention that a first-order gas-liquid transition may be absent in a dusty plasma, as in other strongly coupled plasmas.)

In the experiment of HG [47,48], a 2D dusty plasma was sustained under liquid conditions by using laser heating [86], over a range of kinetic temperatures. The primary purpose of HG was to investigate viscosity, which relied on their use of video microscopy to obtain particle positions in each video frame. We find their particle-position data are well suited for the purpose of obtaining  $S(k)$ , which the original authors HG did not calculate.

Along with these analyses of all the previous experiments, including HG, we also performed new molecular dynamics simulations. These simulations were done with pointlike charged particles, constrained to move on a 2D plane, and interacting with a Yukawa potential. Simulation parameters were chosen to model the dusty plasma liquid experiment of HG, over the same temperature range.

Our chief result is that  $S_{\min}$  was especially small in the dusty plasma liquid experiment of HG. This conclusion is based on a comparison with the other 27 liquid experiments that we reviewed [19,26–46]. The value in a dusty plasma liquid, which we found to be as little as 0.0139, was smaller than in all the other liquid experiments except for some with liquid metals [26], where the uncertainty estimate ranges were too large to allow a definitive conclusion. We found that the

dusty plasma liquid also had one of the smallest values of the ratio  $S_{\min}/S_{\text{peak}}$ , suggesting that choosing a soft interaction may be useful in the path to hyperuniformity. In our analysis of temperature dependence, we found a trend for  $S_{\min}$  to increase with  $T$ . Simulation results were generally consistent with our analysis of the experiment of HG, indicating that the simulation's simple model preserves the most important physics of the experiment. We also obtained a value of the 2D isothermal compressibility for the dusty plasma liquid experiment.

## II. DUSTY PLASMA EXPERIMENT

Since the experiment that we consider in the greatest is the dusty plasma experiment of HG [47,48], we discuss it here. We chose that experiment because it included runs under liquid conditions at multiple temperatures, and it yielded particle-position data that we found to be well suited for our analysis of  $S(k)$ . The conditions of this liquid have been reported in the original papers of HG [47,48] as well as in subsequent analyses of their data to yield autocorrelation functions [88], defect maps [89], and the Einstein frequency [90]. For this liquid, the goals for our present analysis are to characterize values of  $S(k)$  at small  $k$  at different temperatures, and to compare these values with existing experimental literature for other liquids.

The experiment of HG, described in detail in the original reports [47,48], is summarized here. A radio-frequency plasma was formed by partially ionizing room-temperature argon gas at 0.8 Pa pressure. Polymer particles, made of melamine formaldehyde, were used. Their mass was  $M = (5.2 \pm 0.5) \times 10^{-13}$  kg and their diameter was  $8.7 \pm 0.3 \mu\text{m}$ , where the latter value indicates the size dispersion, which is an inherent property of all laboratory dusty plasmas. These polymer particles were introduced into the plasma from above. They then gained a negative charge and became levitated above a negatively biased lower electrode. These particles collected into a round cloud, about 50 mm in diameter, due to horizontal confinement provided by steady weak radial electric fields. We note that a finite size, as in this experiment, is an inherent property of all laboratory dusty plasmas. To constrain the particle cloud to a single horizontal monolayer, so that it can be analyzed as a 2D system, the experimenters used only about 6000 particles, since further addition of particles would have resulted in additional horizontal layers.

The primary diagnostic was video microscopy for measuring the positions and motion of the individual dust particles. A top-view camera recorded images of the particles, as in Fig. 1. Image analysis [78] yielded the particle positions in a video frame, with a subpixel error, as discussed in the Supplemental Material [20]. These measurements were made for all 4096 frames, which were recorded at 70 frames/s. These particle-position measurements also allowed a characterization of the particle motion [91], including their mean-square velocity, to obtain their kinetic temperature  $T$ . Additionally, a side-view camera was used to verify that out-of-plane motion was negligible, and that the layer of dust particles did not buckle, so that it can be analyzed as being 2D.

Before applying laser heating, the dust particles self-organized in a stable triangular crystalline lattice. An analysis

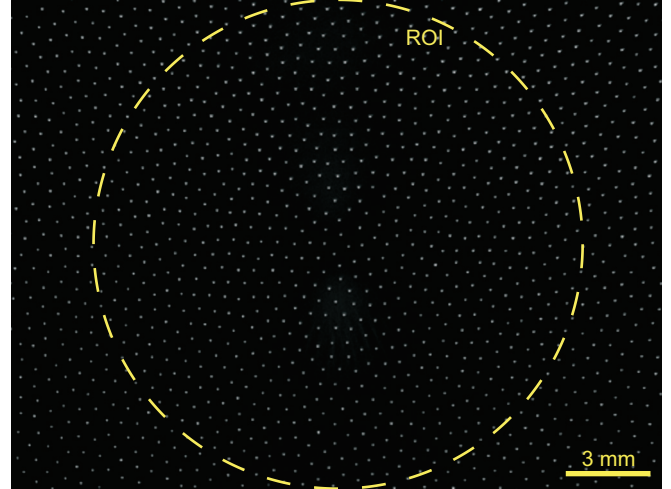


FIG. 1. Example image from the top-view camera, in the experiment of HG [47,48]. The field of view (FOV) was  $23 \times 17$  mm, which was smaller than the diameter of the entire cloud [20]. Individual microparticles appear as white dots that fill multiple pixels. The dashed circle indicates the region of interest (ROI) for our analysis, where the particle density was more uniform than in the corners of the FOV. This image is from the run with  $T/T_m = 1.19$ .

of phonon spectra [92] in this solid phase yielded a measure of the mean charge  $Q = -15\,700 e$  of a dust particle. We note that  $Q$  is proportional to the particle diameter [56], so that the  $\pm 3.4\%$  diameter dispersion leads to a charge dispersion of the same percentage. Other parameters calculated in the experiment include areal number density  $n_d = 3.5 \times 10^6 \text{ m}^{-2}$ , 2D Wigner-Seitz radius  $a = (\pi n_d)^{-1/2} = 0.303 \text{ mm}$ , screening length  $\lambda = 0.421 \text{ mm}$ , screening parameter  $\kappa = a/\lambda = 0.719$ , and a nominal 2D dust plasma frequency  $\omega_{pd} = (Q^2/2\pi\epsilon_0 M a^3)^{1/2} = 89 \text{ s}^{-1}$ . The above quantities, all obtained from recordings of the solid phase, are expected to have the same values in the liquid phase.

By applying laser heating [86], the experimenters melted the crystalline lattice, yielding steady liquid conditions. Eight liquid runs were performed at varying laser intensity, to adjust the kinetic temperature  $T$  over a 31% range, from  $T = 96\,800$  to  $127\,000 \text{ K}$ . We note that the kinetic temperature, for the random movement of dust particles, is different from the much cooler internal temperature of the polymer substance within a particle itself, which remained solid due to immersion in room-temperature gas.

In this paper, we analyze the eight experimental liquid runs without shear. Other runs reported by HG, with sheared velocity that was sustained externally by an additional pair of laser beams, are not analyzed here.

To verify that the conditions were liquid, we compare the measured kinetic temperature to the melting point  $T_m$ . Using the Yukawa crystal's melting point, as expressed by Eq. (3) in Ref. [87], the kinetic temperature range of  $T = 96\,800$ – $127\,000 \text{ K}$  corresponds to a range of  $1.15$ – $1.50 T_m$ . This range also corresponds to  $\Gamma = 139$ – $104$ , where  $\Gamma = Q^2/4\pi\epsilon_0 a k_B T$  is the Coulomb coupling parameter.

Nonequilibrium conditions were present in the experiment of HG, as with most other laboratory plasma experiments. The

underlying causes of nonequilibrium conditions in a laboratory dusty plasma include energy sources and sinks that are external to the plasma and a transfer of energy among plasma components (dust, ions, electrons, and gas), which have different temperatures. Considering a collection of dust particles by itself, the energy sources included laser heating [80,84,86,93] and ion streaming [94,95], while gas friction was an energy sink [55,96]. Despite these intrinsic nonequilibrium conditions, in the experiment of HG, the collection of dust particles had some equilibriumlike properties. In particular, in their microscopic motion the dust particles mimicked molecules in thermal equilibrium, as judged by two tests [47]. First, the velocity distribution was nearly Maxwellian, and second, the temperature fluctuations for a finite-size system were not much more than the theoretical canonical fluctuation level for an equilibrium. This situation, of an intrinsically nonequilibrium system that has microscopic motion mimicking that of an equilibrium, also occurs in experiments with driven granular fluids [97].

As with other dusty plasma experiments, in HG the characteristic spatial and temporal scales were well suited for microscopic observations. The spatial scale, which is particularly important for the static structure factor  $S(k)$ , is characterized by the 2D Wigner-Seitz radius, which had a value of  $a = 0.303$  mm in Refs. [47,48]. Temporal scales can be quantified using correlation times for microscopic motion. In Refs. [88,89], these were of order 100 ms or  $10 \omega_{pd}^{-1}$ . These spatial and temporal scales were well suited for video imaging.

### III. SIMULATION OF THE DUSTY PLASMA EXPERIMENT

A molecular dynamics simulation was also performed, recording the same type of particle-position data as in the experiment of HG [47,48]. Rather than accounting in detail for all the components of a dusty plasma, only the dust particles were simulated. The LAMMPS code [98] was used to model the dynamics of the particles in a microcanonical ensemble.

The simulation parameters and method are described here. The simulation box was  $23 \times 30$  mm, which is somewhat larger than camera's field of view in the experiment, and it contained 2400–2600 particles. Boundary conditions were taken to be periodic. The particles were constrained on a 2D plane and interacted via a repulsive Yukawa potential, which was cut off at a radius of  $20a$ . The dimensionless parameters  $\Gamma$  and  $\kappa$  were chosen to match the experimental values for multiple experimental runs. After the simulation run was initiated, the particles were scattered by collisions and gradually equilibrated. The kinetic temperature was established by a stochastic-velocity-rescale thermostat [99] with a time constant of  $0.2 \omega_0^{-1}$ , where  $\omega_0 = \omega_{pd}/\sqrt{2}$  is a convenient time scale for the simulation. After the desired steady state was attained, the thermostat was turned off. The equation of motion of particles was integrated with a time step of  $0.005 \omega_0^{-1}$ , which was confirmed to provide energy conservation. Particle positions were recorded once every  $\omega_0^{-1}$  over a duration of  $5000 \omega_0^{-1}$ . This protocol allowed recording data for a longer duration than in the experiment, so that the simulation yielded better statistics.

The simulation allows us to test a physical system that resembles the experiment of HG, but with simplified physics. Like the experiment, the simulation had a collection of charged particles interacting through a screened Coulomb interaction. Unlike the experiment, the simulation had identical particles, which moved randomly under thermal equilibrium, and their interparticle forces were described entirely by the Yukawa potential. Factors in the experiment that were not captured in the simulation include: a finite dispersion of particle size and therefore particle charge; nonequilibrium effects mentioned above; weak horizontal electric fields that provided confinement; and a nonuniform density, arising from the confinement, with the greatest density near the center.

### IV. ANALYSIS METHOD

For experiments that rely on imaging as the diagnostic, the calculation of the static structure factor  $S(k)$  can be obtained from the positions  $\mathbf{r}_i(t)$  of  $N$  particles. The particles that we selected as an input for the calculation were those within a circular region of interest (ROI), as shown in Fig. 1 for the experiment of HG. The same procedure was used when analyzing the simulation data, with a circular ROI containing the same number of particles as in the experiment, which ranged from  $N = 820$  to 870, depending on temperature of each experimental run.

Having identified the particle positions that are its input, we next calculated  $S(k, t)$  and then averaged over time to yield  $S(k)$ , using the steps listed here. First, we calculated

$$\rho(\mathbf{k}, t) = \sum_{i=1}^N \exp[i\mathbf{k} \cdot \mathbf{r}_i(t)],$$

which is a dimensionless instantaneous microscopic  $\mathbf{k}$ -space particle density [1]. Its fluctuations are

$$\tilde{\rho}(\mathbf{k}, t) = \rho(\mathbf{k}, t) - \langle \rho(\mathbf{k}, t) \rangle_t.$$

Here, the Fourier-transform variable  $\mathbf{k}$  is a specified input to the calculation, and it has a direction at angle  $\theta$  with respect to the  $x$  axis. We then calculated

$$S(k, t) = N^{-1} \langle \tilde{\rho}(\mathbf{k}, t) \tilde{\rho}^*(\mathbf{k}, t) \rangle_\theta$$

from the positions  $\mathbf{r}_i(t)$  of  $N$  particles [3], where the brackets  $\langle \rangle_\theta$  and  $\langle \rangle_t$  indicate averages over angles and time, respectively, while  $*$  denotes complex conjugate. We chose to average over 360 angles. These calculation steps were for one moment of time, when data were recorded in the experiment or simulation. For subsequent times, we computed  $S(k, t)$  again, to obtain full time series of this dimensionless quantity. Finally, we averaged  $S(k, t)$  over time using at least 4000 sampling times to yield the static structure factor  $S(k)$ .

To identify  $S_{\min}$ , we selected the lowest data point in the  $S(k)$  curve. Although the lowest data point ideally would always be the graph's first data point (i.e., the one with the smallest  $k$ ), in experiments that data point sometimes has an

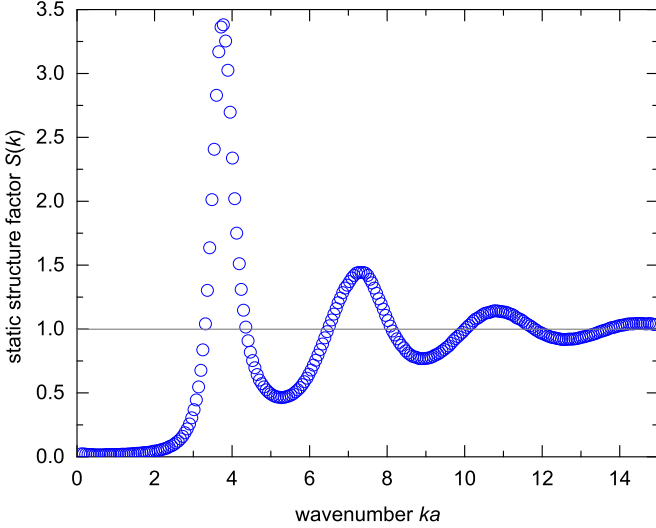


FIG. 2. Static structure factor  $S(k)$  for the experimental run of HG with  $T/T_m = 1.19$ . For this experimental run, the lowest data point in the curve is  $S_{\min} = 0.0154$ , and the height of the first peak (obtained by fitting to a parabola) is  $S_{\text{peak}} = 3.38 \pm 0.01$ . The horizontal axis is normalized by the 2D Wigner-Seitz radius  $a$ .

exaggerated value due to noise or artifacts, as illustrated in the Supplemental Material [20]. For this reason, as a straightforward way of evaluating  $S(k)$  data consistently, for the dusty plasma experiment as well as other experiments in the literature, we simply selected the lowest data point in the  $S(k)$  curve.

We report the value of  $S_{\min}$  along with the ratio  $S_{\min}/S_{\text{peak}}$ , which is our estimate of the hyperuniformity index  $H$ . For this ratio, we obtained  $S_{\text{peak}}$  by selecting  $S(k)$  data points near the first peak and fitting them to a parabola.

## V. RESULTS FOR THE DUSTY PLASMA

### A. Experiment

In our analysis, we obtained the static structure factor  $S(k)$  for all eight liquid runs in the experiment of HG [47,48]. As an example, for the run at  $T/T_m = 1.19$ , our result is shown in Fig. 2. Qualitatively, as with other liquids, the  $S(k)$  curve begins with small values at small  $k$ , followed by a large first peak and then a series of peaks of diminishing heights at large  $k$ . For the run in Fig. 2, the first peak has a height of  $S_{\text{peak}} = 3.38 \pm 0.01$ .

Identifying each curve's lowest data point, we find that  $S_{\min}$  ranged from 0.0139 to 0.0165 in the dusty plasma experiment, in Fig. 3(a), for runs at various temperatures. The run at  $T/T_m = 1.15$  had the lowest value,  $S_{\min} = 0.0139$ . As noted in the Supplemental Material [20], random errors are indicated in Fig. 3(a) by a scatter of  $\pm 2.9\%$  for  $S_{\min}$ .

Dividing the lowest data point  $S_{\min}$  by the height of the first peak  $S_{\text{peak}}$ , we find  $S_{\min}/S_{\text{peak}} = 4.0 \times 10^{-3}$ , as our estimate of the hyperuniformity index  $H$ . The scatter in Fig. 3(a) is  $\pm 3.4\%$  for  $S_{\min}/S_{\text{peak}}$ .

As another result for the experiment of HG, we find a trend for  $S_{\min}$  to increase with temperature. This trend is seen in Fig. 3. There is a 14% increase in  $S_{\min}$  as  $T$  is increased

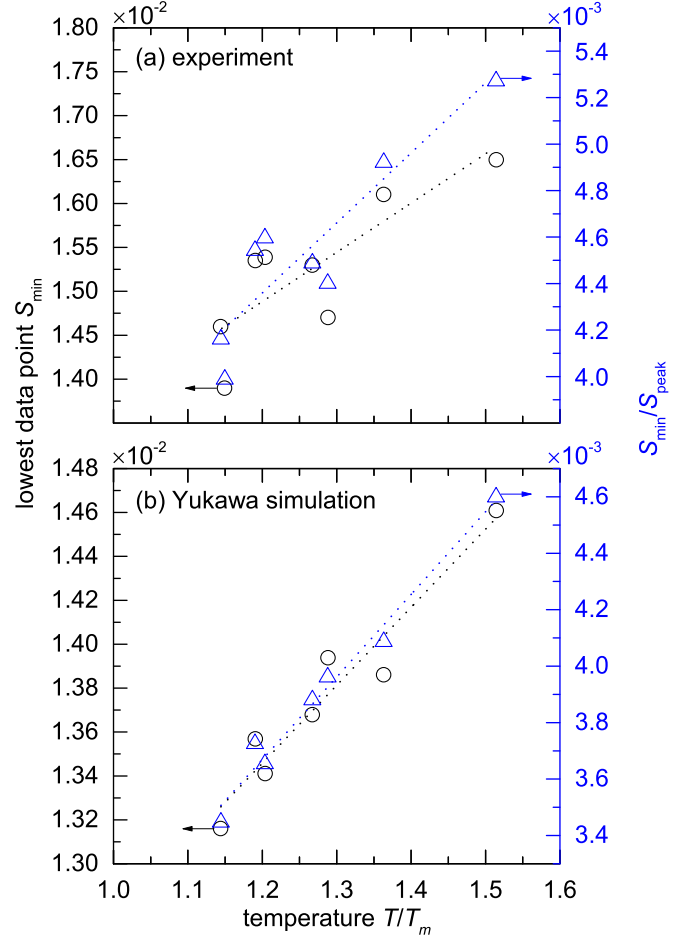


FIG. 3. Lowest value  $S_{\min}$  as a function of temperature  $T/T_m$  for (a) experiment of HG with  $N$  ranging from 820 to 870, depending on  $T/T_m$ , and (b) 2D Yukawa simulation with  $N$  similar to that of the experiment. We find that  $S_{\min}$  has its smallest value near the melting point  $T_m$ . The lowest experimental data point is  $S_{\min} = 0.0139$  at  $T/T_m = 1.15$ . There is an upward trend for  $S_{\min}$  to increase with  $T/T_m$ , as indicated by dotted lines. As our measure of the hyperuniformity index,  $S_{\min}/S_{\text{peak}}$  is also plotted with its values on the right axis. Temperature trends for  $S_{\min}$  and  $S_{\min}/S_{\text{peak}}$  can be seen for both experiment and simulation. Data here are tabulated in the Supplemental Material [20].

from 1.14 to 1.51  $T_m$ , as indicated by a line drawn through the experimental data points in Fig. 3(a).

### B. Simulation

Simulation results for  $S_{\min}$ , shown in Fig. 3(b), are well suited for comparison to the result in Fig. 3(a) for our analysis of the HG experiment. This comparison is aided by the small degree of scatter in the simulation data points. This advantage of the simulation may be due to its longer duration of data recording, and its absence of nonequilibrium phenomena that are present in the experiment.

We find that the simulation results are generally consistent with the experiment. In particular, the presence of a temperature trend for  $S_{\min}$  and the quantitative values of  $S(k)$  at small

$k$  are much alike for the simulation and experiment, as we explain next.

For the temperature trend, we note that, like the experiment, the simulation results exhibit an upward variation of  $S_{\min}$  with temperature. The small degree of scatter of data points in Fig. 3(b) allows us to draw this conclusion with confidence.

Quantitatively, the values of the simulation data points show a near agreement with the experimental data points in Fig. 3. This result is encouraging, as a validation of the simulation, indicating that the most important physics in the experiment has been preserved in the simulation. We do not expect exact agreement of experiment and simulation, as the latter is based on a physical description that is simplified by not including at least four experimental factors, as described in Sec. III.

A finite system size is a topic that can be explored using simulation data. Unlike liquid metals and other physical systems, as analyzed in Sec. VI, a laboratory dusty plasma inherently has a much smaller number of particles, of order  $10^3$ , when the particles themselves are large enough to have thousands of elementary charges as in the experiment of HG. Because finite system size is an unavoidable property of an experimental dusty plasma, the effect of a finite size is mainly of theoretical interest.

While experimental data is the primary focus of this paper, we have used our simulation data to explore the question of whether the existence of the temperature trend is peculiar to one system size. In this test, we varied the area of the ROI for the simulation data. We found that the slope of  $S_{\min}$  vs  $T$  always remained upward, when the system size was varied. Further details are in the Supplemental Material [20].

### C. Isothermal compressibility

The isothermal compressibility is well known to be

$$\chi_T = S(0)/nk_B T,$$

where  $n$  is the number density in three dimensions, or the areal number density in 2D. While  $S(0)$  cannot be measured directly in an experiment, we will approximate its value using an experimental measurement of  $S_{\min}$ .

For the experiment of HG, we calculated that the 2D isothermal compressibility is  $\chi_T = 2.81 \times 10^9 \text{ m}^2/\text{J} = 4.51 \times 10^8 \text{ nm}^2/\text{eV}$ . This value was obtained by combining  $S_{\min} = 0.0139$ , a kinetic temperature  $T = 96\,835 \text{ K}$ , and the very small value of the areal number density  $n = 3.7 \times 10^6 \text{ m}^{-2}$ .

## VI. COMPARISON WITH PREVIOUS EXPERIMENTS

### A. Literature that was surveyed

To compare a 2D dusty plasma liquid with other liquids, we searched the literature for experimental measurements of  $S(k)$  for various substances. We identified 22 previous experimental papers [19,26–46], which included  $S(k)$  as curves or tables that we could analyze to obtain  $S_{\min}$  and  $S_{\text{peak}}$ , using the same consistent approach. Those 22 experimental papers reported a total of 27 experiments. Our compilation of values of  $S_{\min}$  and  $S_{\text{peak}}$  for these previous experiments may have a further use,

beyond our immediate purpose of comparing with the dusty plasma experiment of HG, because it illustrates typical values for various liquids. One reason for interest in these values, especially for  $S(k)$  at small  $k$ , is recent literature regarding hyperuniformity [5–19].

Using data reported in these 22 experimental papers, we obtained values of  $S_{\min}$ . The accuracy of our reading of this value varied somewhat, among the various experiments, due to the way that  $S(k)$  was graphed in the original reports, as we discuss in the Supplemental Material [20].

The substances for the 22 previous experimental papers in our literature survey can be grouped in three categories: liquid metals [26–37], other atomic liquids [38–42], and colloids [19,43–46]. All these substances filled a three-dimensional volume, except for the 2D colloid in Ref. [19]. For our analysis of the 27 experiments reported in these 22 papers,  $S_{\min}$  was found to have a mean value of 0.0706. Values of  $S_{\min}$  lower than that mean value were mostly for liquid metals and some colloids.

The liquid was unsheared in most of these previous experiments, as with the data we analyzed for the dusty plasma experiment of HG. There is a compelling reason to consider sheared liquids separately: when a strong shear is applied, the liquid's microscopic structure can become anisotropic. While detecting this effect of shearing is difficult in atomic liquids, it is easier in colloids [100]. It was found that the peaks and other parts of the  $S(k)$  curve exhibit a variation with respect to direction, in sheared-colloid experiments by Clark and Ackerson [100] and Wilken *et al.* [46]. While we included the latter experimental paper among the 22 that we review, for consistency with our analysis of the other experiments, we used  $S(k)$  curves that were averaged over all directions to obtain the values of  $S_{\min}$  and  $S_{\text{peak}}$  reported in the Supplemental Material [20].

### B. Values of $S_{\min}$

To facilitate a comparison, we combined the 27 previous experiments along with the dusty plasma liquid and sorted them into quartiles according to the value of  $S_{\min}$ , as presented in Table I. The lowest quartile for these papers had  $S_{\min} \leq 0.016$ , while the highest quartile had  $S_{\min} \geq 0.130$ , as shown in Table I. Based on these statistics, we can say that, in general, a typical value of  $S_{\min}$  for a liquid is in a range 0.02–0.13.

We have here an interest in liquids having the smallest values of  $S_{\min}$ , since physically these liquids will correspondingly have low values of isothermal compressibility and hyperuniformity index. For the literature that we surveyed, the lowest quartile of experiments included six liquid-metal experiments [26,28] as well as one experiment with colloid particles [46]. The other five colloid experiments were not among the lowest quartile for  $S_{\min}$ . Likewise, none of the other atomic liquids (He, Kr, and Cl) were among the lowest quartile.

As our chief result, we find that for the dusty plasma liquid, the lowest value of  $S_{\min} = 0.0139$  is especially small in comparison to all these previous experiments with other kinds of liquids. That value is within the lowest quartile, for values of  $S_{\min}$ . Earlier experiments that also fell in the lowest

TABLE I. Summary of  $S_{\min}$  values, for our analysis of previous liquid experiments. The detailed data in Table S-2 of the Supplemental Material [20] are consolidated here and sorted to indicate typical ranges of the value of  $S(k)$  at small  $k$ . In the “substances” column, the liquid metals and other atomic liquids are identified by a chemical symbol, while the abbreviations HG and COL indicate our analysis of the dusty plasma liquid of Haralson and Goree [47,48] and colloid experiments, respectively. It is noteworthy that there are large uncertainty estimates for  $S_{\min}$  in some older liquid metal experiments included in the first quartile of this table; for example, the lowest  $S_{\min}$  value for Pb, 0.0015, has a large uncertainty of  $\pm 0.03$  as reported by the original experimenters [26]. These uncertainty estimates for liquid metals are discussed further in the text.

quartile	range of $S_{\min}$	substances
1 <sup>st</sup>	$S_{\min} \leq 0.016$	Pb [26], Zn [26], HG, Sn [26], Sn [28], Tl [26], COL [46]
2 <sup>nd</sup>	$0.018 \leq S_{\min} \leq 0.031$	Al [32], Ge [31], Ge [30], Na [27], Bi [26], K [27], Tl – Se [33]
3 <sup>rd</sup>	$0.034 \leq S_{\min} \leq 0.073$	Cs [29], COL [45], Li – N [37], COL [44], Pb – K [36], Kr [42], COL [19]
4 <sup>th</sup>	$S_{\min} \geq 0.130$	Cl [40], He [41], COL [44], He [38,39], COL [43], Rb [34], Ga [35]

quartile were mostly done with liquid metals. Some of those liquid-metal experiments yielded values of  $S_{\min}$  lower than for the dusty plasma liquid, but this comparison is complicated by large uncertainty estimates for the liquid metals, as we explain next.

In comparison to our analysis of the dusty plasma liquid in Sec. V, the five liquid-metal experiments that might have smaller experimental values of  $S_{\min}$  are those reported in the 1968 paper by North *et al.* [26]. However, it is impossible to draw a definitive conclusion about which  $S_{\min}$  is the smallest, due to a combination of large uncertainties reported by North *et al.*, and their use of linear-linear graphs. For that paper, our analysis of  $S_{\min}$ , along with  $\pm$  uncertainty values reported in the original paper, are as follows:  $S_{\min} = 0.0015 \pm 0.03$  for Pb,  $0.011 \pm 0.05$  for Zn,  $0.015 \pm 0.03$  for Sn,  $0.015 \pm 0.05$  for Tl, and  $0.029 \pm 0.05$  for Bi. (For two of these liquid metals, various temperatures were reported, and we selected the temperature for which  $S_{\min}$  was the lowest.)

The uncertainty estimates have a wide span, for those five experiments with liquid metals [26]. They are so wide that they overlap with the lowest value of 0.0139 for the dusty plasma liquid. Thus, in comparing the different kinds of liquids, it is impossible to conclude definitively whether one of the metals in the 1968 paper [26] or the dusty plasma liquid actually had the lowest value of  $S_{\min}$ .

### C. Values of $S_{\text{peak}}$ and $S_{\min}/S_{\text{peak}}$

Besides  $S_{\min}$ , we also obtained the height of the first peak,  $S_{\text{peak}}$ , and the ratio  $S_{\min}/S_{\text{peak}}$ , all for the 22 previous experimental papers. We find that the first peak of  $S(k)$  is higher for the 2D dusty plasma liquid than for most other kinds of liquids. For example, for the run in Fig. 2,  $S_{\text{peak}} = 3.38 \pm 0.01$ , while  $S_{\text{peak}}$  has a much lower value in the range of 1.18–3.07 for liquid metals [26–37] and 1.06–2.38 for other atomic liquids [38–42] or colloids [19,43–46].

For the ratio  $S_{\min}/S_{\text{peak}}$ , which serves as our measure of the hyperuniformity index  $H$ , the conclusion we drew above for  $S_{\min}$  also applies to  $S_{\min}/S_{\text{peak}}$ . In particular, the dusty plasma liquid that we analyzed was found to have an especially small value of  $S_{\min}/S_{\text{peak}}$ , as compared with the same 22 previous experimental papers. Among those previous experiments, only for the same five liquid metals [26] might achieve values of  $S_{\min}/S_{\text{peak}}$  lower than for the dusty plasma liquid, but this judgment is again not definitive due to the large uncertainty estimates reported in Ref. [26].

### D. Temperature trend

The temperature trend that we identified in Sec. V for  $S_{\min}$  is already a known phenomenon, but it is perhaps not widely mentioned. Among the 22 experimental papers that we reviewed, in only one did the narrative include a remark upon an increase with temperature, for  $S(k)$  at small  $k$ . That paper [39] was for a liquid helium experiment, where it was noted that, for  $k \lesssim 0.5 \text{ \AA}^{-1}$ ,  $S(k)$  “increases monotonically with increasing temperature.” For a quantum liquid such as helium, this monotonic trend was predicted also theoretically, by thermodynamic arguments that involve isothermal compressibility [39,101]. For other kinds of liquids, mentions of this temperature trend seem to be uncommon.

We can identify this temperature trend in the data reported in some papers, even when the original authors did not comment upon it. In particular, we can mention two of the 22 papers that we reviewed. For liquid Cs, our analysis of  $S(k)$  in Fig. 2 of Ref. [29] revealed that  $S_{\min}$  increased 38% as  $T$  was raised by a factor of 1.4. For liquid helium, we find in the graph of  $S(k)$  in Fig. 1(b) of Ref. [41] that there was a 22% increase in  $S_{\min}$  as the absolute temperature  $T$  was increased fivefold.

In presenting our data, with respect to temperature, we normalized the kinetic temperature by the melting point  $T_m$ . We made this choice motivated by a remark in the 1994 book on liquids, by Balucani and Zoppi [3], that “the very low values of  $S(k \rightarrow 0)$  apparent in {Fig. 2 of Ref. [29]} are typical for all liquids near melting. . .” This comment suggests that cold liquids near the melting point will tend to have smaller values than hotter liquids, for  $S(k)$  at small values of  $k$ . That suggestion is consistent with the temperature trend that we discussed above. Since various substances differ according to their melting points, it is useful to use the normalization  $T/T_m$ , for example in our tables of results in the Supplemental Material [20], to aid comparisons of different substances in liquid form.

## VII. SUMMARY

We obtained  $S(k)$  curves by analyzing data from the dusty plasma liquid experiment of HG [47,48]. We also performed and analyzed a Yukawa molecular dynamics simulation to yield  $S(k)$ . In both the experiment and simulation, the particles moved in a two-dimensional plane. The interparticle interaction was soft, with a long-range electric repulsion. In

analyzing  $S(k)$ , we identified its lowest data point, which we call  $S_{\min}$ . This data point is always found at small  $k$ .

Our chief observation for the dusty plasma experiment is that  $S_{\min}$  had a value as low as 0.0139. We judge this value to be especially small by carrying out a comparison with previous experiments.

This comparison to previous experiments is based on our search of the literature for  $S(k)$  measurements in liquid metals, other atomic liquid, and colloids. In this search, we identified experiments that yielded  $S(k)$  measurements that we could consistently analyze using the same approach of identifying the lowest data point,  $S_{\min}$ . The overall number of experiments we reviewed was 27, as reported in 22 separate papers [19,26–46]. Sorting the values of  $S_{\min}$  for these 27 previous experiments, we find that, in general,  $S_{\min}$  tends to be in a range from 0.02 to 0.13 for a liquid. We would expect  $S(0)$  to have similar values.

The outcome of this comparison is that the dusty plasma liquid has an especially small value of  $S_{\min}$ . In fact, for only five liquid-metal experiments, all reported in the paper by North *et al.* [26], is it possible that  $S_{\min}$  had a lower value than we found for the dusty plasma liquid experiment. However, that comparison to North *et al.* is not definitive due to the large uncertainty estimates for  $S(k)$  reported by the original authors [26]. In other words, there is a possibility that a dusty plasma liquid could have a lower value of  $S_{\min}$  than for any of the liquid substances we surveyed.

An additional result from our analysis of the dusty plasma liquid experiment was identifying a distinctive temperature trend, for  $S_{\min}$  to increase with  $T$ . This trend for  $S(k)$  at small  $k$  was already known [3,39], but not often mentioned, in the literature for other liquids.

Our molecular dynamics simulation was designed to model the dusty plasma experiment of HG, with simplified physics. Parameters for the interparticle interaction and system size were comparable to those of the experiment. Even though several factors present in the experiment were not included in

the simulation, its results were consistent with the experiment, including the trend for  $S_{\min}$  to increase with temperature  $T$ .

Our results for  $S(k)$  at small  $k$  are relevant for two kinds of physical properties, compressibility and hyperuniformity. The isothermal compressibility  $\chi_T$  is proportional to  $S(0)$ , but the latter quantity cannot be measured directly in an experiment. Approximating  $S(0)$  by  $S_{\min}$ , we calculated a compressibility of  $2.81 \times 10^9 \text{ m}^2/\text{J}$ , for the run at  $T = 1.15 T_m$  in the dusty plasma liquid experiment of HG.

Perfect hyperuniformity is an idealized theoretical condition, where  $S(k \rightarrow 0)$  in a condensed material approaches zero. Recently, there has been an extensive interest in developing design rules for creating effectively hyperuniform materials [5,7,9,10,12–15] for a wide range of proposed applications [5]. For this purpose, the hyperuniformity literature relies on a parameter called the hyperuniformity index [5,51],  $H \equiv S(0)/S_{\text{peak}}$ . As an experimentally practical measure of this hyperuniformity index, we calculated the ratio  $S_{\min}/S_{\text{peak}}$ . For the dusty plasma experiment, we found that this ratio was as small as  $4.0 \times 10^{-3}$ , which is lower than for the liquids in most of the 22 previous experimental papers that we reviewed. Only in the same five liquid-metal experiments [26] could  $S_{\min}/S_{\text{peak}}$  have been lower than for the dusty plasma liquid. This comparison supports the earlier suggestion that materials with soft interparticle interactions should provide a path towards creating real materials that are effectively hyperuniform [7,102].

#### ACKNOWLEDGMENTS

Work at Iowa and Michigan was supported by the Army Research Office, W911NF-18-1-0240. Work at Iowa was also supported by the U.S. Department of Energy (US), DE-SC0014566 and NASA-JPL Subcontracts No. 1573629, No. 1663801, and No. 1672641. We thank Jorge Berumen, John Bollinger, Neeraj Chaubey, Alexandros Chremos, Bin Liu, Sam Wilken, and our MURI team for helpful discussions.

- 
- [1] J.-P. Hansen and I. R. McDonald, *Theory of Simple Liquids* (Elsevier Academic Press, New York, 1986)
  - [2] J.-P. Boon and S. Yip, *Molecular Hydrodynamics* (Dover Publications, New York, 1991).
  - [3] U. Balucani and M. Zoppi, *Dynamics of the Liquid State* (Oxford University Press, New York, 1994).
  - [4] S. Torquato and F. H. Stillinger, *Phys. Rev. E* **68**, 041113 (2003).
  - [5] S. Torquato, *Phys. Rep.* **745**, 1 (2018).
  - [6] G. Zhang, F. H. Stillinger, and S. Torquato, *Sci. Rep.* **6**, 36963 (2016).
  - [7] A. Chremos and J. F. Douglas, *Ann. Phys. (NY)* **529**, 1600342 (2017).
  - [8] F. Martelli, S. Torquato, N. Giovambattista, and R. Car, *Phys. Rev. Lett.* **119**, 136002 (2017).
  - [9] D. Chen, E. Lomba, and S. Torquato, *Phys. Chem. Chem. Phys.* **20**, 17557 (2018).
  - [10] A. Chremos and J. F. Douglas, *Phys. Rev. Lett.* **121**, 258002 (2018).
  - [11] G. Rumi, J. Aragón Sánchez, F. Elías, R. Cortés Maldonado, J. Puig, N. R. Cejas Bolecek, G. Nieva, M. Konczykowski, Y. Fasano, and A. B. Kolton, *Phys. Rev. Res.* **1**, 033057 (2019).
  - [12] G. Zhang and S. Torquato, *Phys. Rev. E* **101**, 032124 (2020).
  - [13] A. Chremos, *J. Chem. Phys.* **153**, 054902 (2020).
  - [14] Z. Ma, E. Lomba, and S. Torquato, *Phys. Rev. Lett.* **125**, 068002 (2020).
  - [15] D. Chen, Y. Zheng, L. Liu, G. Zhang, M. Chen, Y. Jiao, and H. Zhuang, *Proc. Natl. Acad. Sci. USA* **118**, e2016862118 (2021).
  - [16] S. Mitra, A. D. S. Parmar, P. Leishangthem, S. Sastry, and G. Foffi, *J. Stat. Mech.* **2021**, 033203 (2021).
  - [17] S. Torquato, *Phys. Rev. E* **103**, 052126 (2021).
  - [18] D. Chen, Y. Zheng, C.-H. Lee, S. Kang, W. Zhu, H. Zhuang, P. Y. Huang, and Y. Jiao, *Phys. Rev. B* **103**, 224102 (2021).
  - [19] U. S. Nizam, G. Makey, M. Barbier, S. S. Kahraman, E. Demir, E. E. Shafiq, S. Galioglu, D. Vahabli, S. Hüsniügil, M. H. Güneş, E. Yelesti, and S. Ilday, *J. Phys.: Condens. Matter* **33**, 304002 (2021).



- [20] See Supplemental Material at <http://link.aps.org/supplemental/10.1103/PhysRevE.106.055212> for tabulated data of  $S_{\min}$ ,  $S_{\text{peak}}$ , and  $S_{\min}/S_{\text{peak}}$  obtained from our analysis of previously published experiments. The Supplemental Material also contains discussion of the static structure factor for the 2D Yukawa simulation, discussion of methods and uncertainties in the dusty plasma experiment, as well as additional details about crystalline conditions before melting. The Supplemental Material includes Refs. [21–25].
- [21] E. W. Fischer, *Physica A* **201**, 183 (1993).
- [22] V. Vyas, G. A. Hebner, and M. J. Kushner, *J. Appl. Phys.* **92**, 6451 (2002).
- [23] N. Xu and E. S. C. Ching, *Soft Matter* **6**, 2944 (2010).
- [24] R. Kurita and E. R. Weeks, *Phys. Rev. E* **84**, 030401(R) (2011).
- [25] J. R. Rumble, ed., Melting, boiling, triple, and critical point temperatures and densities of the elements, in *CRC Handbook of Chemistry and Physics* (CRC Press/Taylor & Francis, Internet Version, Boca Raton, 2022), 103rd ed.
- [26] D. M. North, J. E. Enderby, and P. A. Egelstaff, *J. Phys. C: Solid State Phys.* **1**, 1075 (1968).
- [27] A. J. Greenfield, J. Wellendorf, and N. Wisser, *Phys. Rev. A* **4**, 1607 (1971).
- [28] D. Jović and I. Padureanu, *J. Phys. C: Solid State Phys.* **9**, 1135 (1976).
- [29] M. J. Huijben and W. van der Lugt, *J. Phys. F: Met. Phys.* **6**, L225 (1976).
- [30] M. Davidović, M. Stojić, and D. Jović, *J. Phys. C: Solid State Phys.* **16**, 2053 (1983).
- [31] P. S. Salmon, *J. Phys. F: Met. Phys.* **18**, 2345 (1988).
- [32] S. Takeda, S. Harada, S. Tamaki, and Y. Waseda, *J. Phys. Soc. Jpn.* **60**, 2241 (1991).
- [33] T. Usuki, Y. Shirakawa, and S. Tamaki, *J. Phys. Soc. Jpn.* **61**, 2805 (1992).
- [34] R. Winter, C. Pilgrim, F. Hensel, C. Morkel, and W. Gläser, *J. Non-Cryst. Solids* **156–158**, 9 (1993).
- [35] S. N. Rapeanu and I. Padureanu, *Phys. Scr.* **T57**, 18 (1995).
- [36] N. M. Blagoveshchenskii, V. A. Morozov, A. G. Novikov, V. V. Savostin, A. L. Shimkevich, and I. Y. Shimkevich, *Phys. B: Condens. Matter* **364**, 255 (2005).
- [37] N. M. Blagoveshchenskii, V. A. Morozov, A. G. Novikov, V. V. Savostin, D. V. Savostin, and A. L. Shimkevich, *Crystallog. Rep.* **53**, 14 (2008).
- [38] V. F. Sears, E. C. Svensson, A. D. B. Woods, and P. Martel, The static structure factor and pair correlation function for liquid  $^4\text{He}$  at saturated vapour pressure, Tech. Rep. AECL-6779, Atomic Energy of Canada Limited, 1979.
- [39] E. C. Svensson, V. F. Sears, A. D. B. Woods, and P. Martel, *Phys. Rev. B* **21**, 3638 (1980).
- [40] J. D. Sullivan and P. A. Egelstaff, *Chem. Phys.* **89**, 167 (1984).
- [41] W. Montfrooij, L. A. de Graaf, P. J. van den Bosch, A. K. Soper, and W. S. Howells, *J. Phys.: Condens. Matter* **3**, 4089 (1991).
- [42] F. Barocchi, P. Chieux, R. Magli, L. Reatto, and M. Tau, *J. Phys.: Condens. Matter* **5**, 4299 (1993).
- [43] R. Krause, B. D'Aguzzo, J. M. Mendez-Alcaraz, G. Nagele, R. Klein, and R. Weber, *J. Phys.: Condens. Matter* **3**, 4459 (1991).
- [44] E. E. Maier, R. Krause, M. Deggelmann, M. Hagenbüchle, and R. Weber, *Macromolecules* **25**, 1125 (1992).
- [45] R. Kurita and E. R. Weeks, *Phys. Rev. E* **82**, 011403 (2010).
- [46] S. Wilken, R. E. Guerra, D. J. Pine, and P. M. Chaikin, *Phys. Rev. Lett.* **125**, 148001 (2020).
- [47] Z. Haralson and J. Goree, *Phys. Plasmas* **23**, 093703 (2016).
- [48] Z. Haralson and J. Goree, *Phys. Rev. Lett.* **118**, 195001 (2017).
- [49] J. N. Tan, J. J. Bollinger, B. Jelenkovic, and D. J. Wineland, *Phys. Rev. Lett.* **75**, 4198 (1995).
- [50] R. Xie, G. G. Long, S. J. Weigand, S. C. Moss, T. Carvalho, S. Roorda, M. Hejna, S. Torquato, and P. J. Steinhardt, *Proc. Natl. Acad. Sci. USA* **110**, 13250 (2013).
- [51] S. Atkinson, G. Zhang, A. B. Hopkins, and S. Torquato, *Phys. Rev. E* **94**, 012902 (2016).
- [52] P. Shukla and A. Mamun, *Introduction to Dusty Plasma Physics* (Institute of Physics Publishing, Bristol, 2001).
- [53] P. M. Bellan, Dusty plasmas, in *Fundamentals of Plasma Physics* (Cambridge University Press, New York, 2006), Chap. 17.
- [54] M. Bonitz, C. Henning, and D. Block, *Rep. Prog. Phys.* **73**, 066501 (2010).
- [55] A. Melzer, *Physics of Dusty Plasmas: An Introduction* (Springer Nature, Cham, 2019).
- [56] E. C. Whipple, *Rep. Prog. Phys.* **44**, 1197 (1981).
- [57] U. Konopka, G. E. Morfill, and L. Ratke, *Phys. Rev. Lett.* **84**, 891 (2000).
- [58] G. Kalman, ed., *Strongly Coupled Plasmas* (Plenum Press, New York, 1978).
- [59] S. Ichimaru, *Rev. Mod. Phys.* **54**, 1017 (1982).
- [60] M. S. Murillo, *Phys. Plasmas* **11**, 2964 (2004).
- [61] T. Ott, M. Bonitz, L. Stanton, and M. Murillo, *Phys. Plasmas* **21**, 113704 (2014).
- [62] H. Thomas, G. E. Morfill, V. Demmel, J. Goree, B. Feuerbacher, and D. Möhlmann, *Phys. Rev. Lett.* **73**, 652 (1994).
- [63] Y. Hayashi and K. Tachibana, *Jpn. J. Appl. Phys.* **33**, L804 (1994).
- [64] R. A. Quinn, C. Cui, J. Goree, J. B. Pieper, H. Thomas, and G. E. Morfill, *Phys. Rev. E* **53**, R2049 (1996).
- [65] K. Takahashi, Y. Hayashi, and K. Tachibana, *Jpn. J. Appl. Phys.* **38**, 4561 (1999).
- [66] J. A. Bittencourt, *Fundamentals of Plasma Physics* (Pergamon Press, New York, 1986).
- [67] F. F. Chen, *Introduction to Plasma Physics and Controlled Fusion* (Springer, New York, 2015).
- [68] Y. Feng, J. Goree, and B. Liu, *Phys. Rev. Lett.* **109**, 185002 (2012).
- [69] M. Baus and J.-P. Hansen, *Phys. Rep.* **59**, 1 (1980).
- [70] G. S. Dubey and D. K. Chaturvedi, *physica status solidi (b)* **108**, 123 (1981).
- [71] J.-L. Bretonnet and A. Derouiche, *Phys. Rev. B* **38**, 9255 (1988).
- [72] S. Nunomura, J. Goree, S. Hu, X. Wang, and A. Bhattacharjee, *Phys. Rev. E* **65**, 066402 (2002).
- [73] Z. Donkó, P. Hartmann, and J. Goree, *Mod. Phys. Lett. B* **21**, 1357 (2007).
- [74] Y. Feng, J. Goree, and B. Liu, *Phys. Rev. Lett.* **105**, 025002 (2010).
- [75] J. K. Meyer, I. Laut, S. K. Zhdanov, V. Nosenko, and H. M. Thomas, *Phys. Rev. Lett.* **119**, 255001 (2017).
- [76] N. P. Kryuchkov, E. V. Yakovlev, E. A. Gorbunov, L. Couëdel, A. M. Lipaev, and S. O. Yurchenko, *Phys. Rev. Lett.* **121**, 075003 (2018).

- [77] F. Wieben and D. Block, *Phys. Rev. Lett.* **123**, 225001 (2019).
- [78] Y. Feng, J. Goree, and B. Liu, *Rev. Sci. Instrum.* **78**, 053704 (2007).
- [79] Y.-J. Lai and L. I, *Phys. Rev. Lett.* **89**, 155002 (2002).
- [80] B. Liu and J. Goree, *Phys. Rev. Lett.* **100**, 055003 (2008).
- [81] Y.-S. Su, C.-W. Io, and L. I, *Phys. Rev. E* **86**, 016405 (2012).
- [82] B. Liu, J. Goree, and O. S. Vaulina, *Phys. Rev. Lett.* **96**, 015005 (2006).
- [83] H. Löwen, C. P. Royall, A. Ivlev, and G. E. Morfill, *AIP Conf. Proc.* **1397**, 201 (2011).
- [84] M. Wolter and A. Melzer, *Phys. Rev. E* **71**, 036414 (2005).
- [85] V. Nosenko, J. Goree, and A. Piel, *Phys. Plasmas* **13**, 032106 (2006).
- [86] Z. Haralson and J. Goree, *IEEE Trans. Plasma Sci.* **44**, 549 (2016).
- [87] P. Hartmann, G. J. Kalman, Z. Donkó, and K. Kutasi, *Phys. Rev. E* **72**, 026409 (2005).
- [88] Z. Haralson, J. Goree, and R. Belousov, *Phys. Rev. E* **98**, 023201 (2018).
- [89] C.-S. Wong, J. Goree, and Z. Haralson, *Phys. Rev. E* **98**, 063201 (2018).
- [90] C.-S. Wong, J. Goree, and Z. Haralson, *IEEE Trans. Plasma Sci.* **46**, 763 (2018).
- [91] Y. Feng, J. Goree, and B. Liu, *Rev. Sci. Instrum.* **82**, 053707 (2011).
- [92] S. Nunomura, J. Goree, S. Hu, X. Wang, A. Bhattacharjee, and K. Avinash, *Phys. Rev. Lett.* **89**, 035001 (2002).
- [93] B. Liu, J. Goree, and Y. Feng, *Phys. Rev. E* **78**, 046403 (2008).
- [94] A. Barkan and R. L. Merlino, *Phys. Plasmas* **2**, 3261 (1995).
- [95] A. Kananovich and J. Goree, *Phys. Plasmas* **27**, 113704 (2020).
- [96] B. Liu, J. Goree, V. Nosenko, and L. Boufendi, *Phys. Plasmas* **10**, 9 (2003).
- [97] M. D. Shattuck, R. A. Ingale, and P. M. Reis, *AIP Conf. Proc.* **1145**, 43 (2009).
- [98] S. Plimpton, *J. Comput. Phys.* **117**, 1 (1995).
- [99] G. Bussi, D. Donadio, and M. Parrinello, *J. Chem. Phys.* **126**, 014101 (2007).
- [100] N. A. Clark and B. J. Ackerson, *Phys. Rev. Lett.* **44**, 1005 (1980).
- [101] P. J. Price, *Phys. Rev.* **94**, 257 (1954).
- [102] W. Wu, M. Singh, A. Masud, X. Wang, A. Nallapaneni, Z. Xiao, Y. Zhai, Z. Wang, T. Terlier, M. Bleuel, G. Yuan, S. K. Satija, J. F. Douglas, K. Matyjaszewski, M. R. Bockstaller, and A. Karim, *Am. Chem. Soc. Nano* **15**, 12042 (2021).